Multifunctional SA-PProDOT Binder for Lithium Ion Batteries

Min Ling, † , // Jingxia Qiu, † Sheng Li, † Cheng Yan, ‡ Milton J. Kiefel,§ Gao Liu,*, // and Shanqing Zhang*, †

† Centre for Clean Environment and Energy, Environmental Futures Research Institute and Griffith School of Environment, Griffith University, Gold Coast Campus, Queensland 4222, Australia
‡ School of Chemistry, Physics and Mechanical Engineering, Queensland University of Technology, Brisbane, Queensland 4001, Australia
§ Institute for Glycomics, Griffith University, Gold Coast Campus, Queensland 4222, Australia
// Environmental Energy Technologies Division, Lawrence Berkeley National Laboratory, Berkeley, California 94720, United States

ABSTRACT

An environmentally benign, highly conductive, and mechanically strong binder system can overcome the dilemma of low conductivity and insufficient mechanical stability of the electrodes to achieve high performance lithium ion batteries (LIBs) at a low cost and in a sustainable way. In this work, the naturally occurring binder sodium alginate (SA) is functionalized with 3, 4-propylenedioxythiophene-2,5-dicarboxylic acid (ProDOT) via a one-step esterification reaction in a cyclohexane/dodecyl benzenesulfonic acid (DBSA)/water microemulsion system, resulting in a multifunctional polymer binder, that is, SA-PProDOT. With the synergetic effects of the functional groups (e.g., carboxyl, hydroxyl, and ester groups), the resultant SA-PProDOT polymer not only maintains the outstanding binding capabilities of sodium alginate but also enhances the mechanical integrity and lithium ion diffusion coefficient in the $LiFePO_4$ (LFP) electrode during the operation of the batteries. Because of the conjugated network of the PProDOT and the lithium doping under the battery environment, the SA-PProDOT becomes conductive and matches the conductivity needed for $LiFePO_4$ LIBs. Without the need of conductive additives such as carbon black, the resultant batteries have achieved the theoretical specific capacity of $LiFePO_4$ cathode (ca. 170 mAh/g) at C/10 and ca. 120 mAh/g at 1C for more than 400 cycles.

KEYWORDS: Binders, multifunctions, conductivities, lithium ion phosphate, lithium ion battery

Lithium ion batteries (LIBs), commercially released for the first time by SONY and Asahi Kasei Corporation in 1991, have become the main power sources for mobile electronics and large scale emerging applications, including various types of electric vehicles (EVs) and energy storage for utility grids. However, despite their widespread application, it remains a formidable challenge in developing high-performance battery system without compromising stability, cost and safety standards. Enormous efforts have been devoted toward the optimization of battery components in order to address these issues. Besides other elemental parts of LIBs, for example, active materials, electrolyte, and membrane, the binder is equally crucial in maintaining conductivity and battery performance.[1,2,3] Polyvinylidene fluoride (PVDF) is a traditional binder that exhibits excellent binding ability and meets the requirements of chemical and electrochemical stability. A limitiation of PVDF is that it is not conductive. This means that in a typical electrode fabrication process, a conductive additive such as carbon black must be added to PVDF in order to improve the electronic conductivity of the electrode at the cost of the energy density and the binding strength of binder.[4–6] The stability of the resultant electrodes and the energy density of the electrode associated with PVDF have been the major barrier to the emergence of improved LIB technologies. Although large amounts of electro-active materials have already been developed, not many of them can be adopted in the market due to these reasons. Therefore, the development of a new highly efficient binder system with multifunctions (e.g., binding capabilities, tolerance of volume expansion, electronic and lithium ion conductivity) to facilitate high energy density LIBs is much more significant than

ever before.[4,7−9] Thus, binders with the tailored electronic and ionic conductivity are desirable to achieve high energy density LIBs in that the conductive additives such as carbon black are no longer needed and the percentage of active materials is improved accordingly. Overall, a binder system with a strong mechanical binding property, stable chemical and electrochemical stability, and satisfactory lithium ion and electronic conductivity is highly desirable for LIBs production.[10,11]

In the 21st century, the identification, modification, and application of natural products in the design and production of energy storage devices has attracted tremendous interest as they are sustainable and commonly low cost.[6,12] PVDF can be considered as a nonsustainable product as it is manufactured through fluorine chemical industry. As a consequence, natural binders such as carboxyl methylated cellulose (CMC) and sodium alginate (SA) polymers have the potential to overcome the aforementioned drawbacks of PVDF as they open up renewable processes for LIBs electrode manufacturing.[13,14] Compared with synthetic polymers, natural polymers have many inherent advantages such as abundance, low cost, and sustainability in the natural world. Moreover, the dispersion and distribution properties of natural polymers are much better than conventional PVDF polymer binder.[15] In contrast to CMC, SA has excellent mechanical properties and a wider range of chemical functionality that provides reaction sites for incorporating additional functional groups or modifying the existing functionality. SA consists of 1−4 linked β-D-mannuronic acid (M) and α-L-guluronic acid (G) as shown in Scheme 1.6,12 Similar to other conventional binders, SA is nonconductive. Among the various approaches to overcome the adverse effects of the poor conductivity,[16–23] low cost and conductive binding systems are a the most practical and economic approach.[4,5,24,25] Fortunately, reactive functional groups such as hydroxyl and carboxylic groups within SA allows it to react with conducting conjugated compounds, such as 3,4-propylenedioxythiophene-2,5-dicarboxylic acid (Pro-DOT). It is founded that pz-orbitals of the conjugated bonds could form long-range π-orbitals that facilitate electron transfer.[4,5] The electronic conductivity can be further enhanced by an in situ lithium doping during charge/discharge of LIBs.[5] Functionalization processes of binders are commonly conducted in organic solvent with complex reaction catalysts and subsequent sophisticated separation procedures.[4,5,24] Here, we present a simple one-step esterification method to integrate ProDOT into the SA framework in a cyclohexane/DBSA/water microemulsion system. Because the hydrophilic and hydrophobic ends of dodecyl benzenesulfonic acid (DBSA) are oriented accordingly, a spherical microemulsion is formed, as shown in Supporting Information Figure S1. The formation of the microemulsion and the evolution of the water droplet can be visually observed under an optical microscopy as shown in Figure S1. Due to the extraction of water generated from condensation, the average diameter of the droplets increase from ca. 15 μm (Figure S1a) to ca. 75 μm (Figure S1b) after the extraction of water generated from condensation. The water−oil interface is clearly demonstrated in Supporting Information Figure S1c. According to our measurement, the pH value of the reaction media is ca. 7.0. Because the pKa value of SA is in the range of 3.4 to 4.4,[26] the carboxylic groups of alginate are mainly in the deprotonated state as shown in Scheme 1.

The ultimate goal of this work is to incorporate conducting functionality to a naturally occurring binder. However, it is challenging to incorporate other functional groups onto the SA backbone while maintaining the advantages of the natural binding capabilities of SA. The resultant microemulsion is homogeneous and semitransparent. After the addition of SA and ProDOT, the turbidity of the microemulsion was increased. A viscous and cream-like colloid was generated after reflux and vigorous stirring in the microemulsion system for 24 h. The resultant product was obtained after evaporation of the solvents in a rotary evaporator. As a surfactant, DBSA can form a thermodynamic stable microemulsion system with hydrophobic phase (external oil phase) and hydrophilic phase (e.g., internal aqueous phase). The ProDOT molecules are mainly distributed in the oil phase with the hydrophilic functional groups −COOH assembly toward the aqueous, whereas alginates are in the aqueous phase with the hydroxyl (−OH) functional group line up toward the oil phase. It is well established that DBSA is an effective catalyst for esterification reaction.[27–29] Under

the above directional arrangement, catalytic functions of DBSA and sufficient temperature, the esterification reaction takes place (Figure 1). One of the important features of the microemulsion system lies in the fact that the water molecules produced from the esterification reaction can be extracted into the droplets due to hydrophilic nature of the interior aqueous domain. This favors the formation of ester bonds and high production yield as the byproduct water of the esterification reaction is removed from the reaction system. As a result the ProDOT is grafted onto the alginate framework. Also, polymerizations among ProDOT molecules and the grafted ProDOT molecules can lead to the formation of a conjugated polymer structure, that is, poly ProDOT (PProDOT).[30,31] As shown in Figure 1 and Scheme 1, the PProDOT block is interlinked with alginate via the ester groups. Within this polymer, alginate can serve as both counterion and an excellent charge compensator in SAPProDOT and consequently facilitate charge transport. Meanwhile, because the deprotonated alginate is more likely protected in the aqueous phase, it is expected that the functional groups such as carboxylate[32−34] in alginate framework is preserved in the esterification and therefore the strong binding capability is maintained. This reaction system has numerous advantages over traditional organic synthesis reactions:[35−37] (i) high yield can be achieved at room temperature (RT) without using oxidative and corrosive acid, basic catalysts, or expensive enzyme catalysts; (ii) removal of the tedious and costly separation process of catalyst after the synthesis reaction; (iii) mild reaction condition also minimizes the production of byproducts and unnecessary waste. Lithium iron phosphate (LFP) has been considered a promising cathode material that could move toward more intensive use of EVs due to its low cost, safety, and high theoretical capacity (170 mAh/g).1,38 In order to demonstrate the effectiveness and practical potentials of the proposed binder, LFP was selected as the cathode material as it has inherently low electronic conductivity (10−9−10−10 S/cm)[39] and Li-ion conductivity (10−14−10−15 cm2/s).[40−44] The electrochemical and mechanical performances of the LFP electrodes fabricated with PVDF, SA and SA-PProDOT binders were also evaluated and compared. In order to quantitatively examine the product SA-PProDOT obtained from the SA and ProDOT condensation reaction. Xray photoelectron spectroscopy (XPS) was conducted as shown in Figure 2a and 2b, where the peaks were fitted by a Gaussian-Lorenz function. As shown in the spectra, the oxygen 1s peak region of SA and the SA-PProDOT were performed separately. The content of O・C・O group at around 289.00 eV increases from 6.48 atom % to 12.57 atom % after the condensation reaction. Meanwhile, the intensity of C・OH group at around 286.50 eV suggests that the hydroxyl group decreases from 35 atom % to 30.92 atom %. Taken together, the decrease of the hydroxyl groups and increase of ester groups clearly indicate that esterification takes place in the microemulsion system Hence, the unreacted 30.92 atom % hydroxyl groups in SAPProDOT maintain the properties of SA, whereas the conjugated structure with ester groups (12.57 atom %) could promote the performance of SA-PProDOT-based LFP electrodes (LFP@SA-PProDOT).[45] The Fourier transform infrared spectroscopy (FTIR) shown in Figure 2c provides further evidence of the chemical nature of the product SA-PProDOT. In the spectrum of SA, the carboxylate anion has two strongly coupled C・O bonds with bond strengths intermediate between C・O and C・O. The carboxylate ion gives rise to two bands: a strong asymmetrical stretching band near 1650−1550 cm−1 and a weaker symmetrical stretching band near 1400 cm−1 as indicated. In the spectrum of SA-PProDOT, the C・O stretching vibrations of esters actually consist of two asymmetrical coupled vibrations: C・C・(・O)・C and O・C・C; these absorption bands occur in the region of 1300−1000 cm−1. The carboxylic acid dimers display the O・H stretching absorption in the region 3300−2500 cm−1, which usually centers near 3000 cm−1 and overlap with the C・H vibration. The conjugated C・O stretch appears at ca. 1700 cm−1 and C・O stretch of the ester group at ca. 1300 cm−1 confirms the successful condensation of SA and ProDOT.[46,47] A series of coin-type half-cells that employ Li metal as both the reference and counter electrodes were tested by galvanostatic measurements in order to investigate the effect of the SA inspired conductive binder (SA-PProDOT) on the electrochemical performance based on LFP electrodes. Meanwhile, SA, SA plus carbon black (SA-

CB), and PVDF plus carbon black (PVDF-CB) binder systems were applied to fabricate LFP electrodes using the identical procedure as control samples. The SEM observations (Supporting Information Figure S2) demonstrate typical distributions of LFP particles with SA-PProDOT and SA-CB binder systems. The conductivity of the SA-CB samples relies on the "bridges" among the CB aggregates. In contrast, the SA-PProDOT binder system can keep both electrical and mechanical integrity of the electrode during the battery cycle without the need of the "bridges".[48] Figure 3a shows cycle performance of LFP electrodes between 2.0 and 4.2 V limits, in half cell configuration. The SA-PProDOT-based LFP electrodes can deliver a theoretical capacity of 172 mAh/g in the first cycle at C/10 charge and discharge rates. As the current density gradually increase to C/2, 1C, and 2C, the reversible capacity of SA-PProDOT-based electrodes are slightly reduced to ca. 163, 143, and 125 mAh/g, respectively. It is interesting to note that the capacity can recover with no fading correspondingly when the current density returns to C/2 and 1C rate. In contrast, SACB binder system-based electrodes show a lower specific capacity than SA-PProDOT-based electrodes especially in high C rate. During the following 400 cycles at 1C rate (Figure 3b), the SA-PProDOT-based electrodes showed excellent capacity retention of 86.6%. The reversible capacity of SA-CB binder system-based electrodes are ca. 130, 120, and 70 mAh/g at the current density of C/2, 1C, and 2C, respectively (Figure 3a) . In contrast, SA-PProDOT electrodes have substantially improved capacity and stability. In addition, the performances of SA based electrodes are detailed in Supporting Information Figure S3. The capacity of the SA-based electrodes decreases continuously without the addition of carbon black and functionalization. The specific capacity is ca. 100, 50, and 10 mAh/g at C/2, 1C, and 2C, respectively. In contrast to the profile in Supporting Information Figure S4, the PVDF-CBbased electrodes, even with the addition of CB conductive additives, the attainable capacity is still lower than SAPProDOT sample. The specific capacity is ca. 145, 130, and 110 mAh/g at C/2, 1C, and 2C, respectively. This can be ascribed to the improvement in not only the electronic conductivity but also the ionic conductivity and higher binding capacity of the as-developed multifunctional SA-PProDOT binder system. In general, upon increasing C rates, the main factor of capacity loss is a higher ohmic drop (signifying low electronic conductivity) that limited Li-ion diffusion in the electrolyte filling the electrode pores. As shown in Figure 3c, the discharge voltage plateau of the LFP electrode is observed at 3.4 V for SA-PProDOT-based electrode. The slight decrease of the LFP discharge voltage plateau based on SA-CB electrode (3.35 V) and SA electrode (below 3.3 V) indicates that the overall performance, (e.g., electronic conductivity, Li-ion diffusion capability) of the PorDOT-SA (3.4 V)-based electrode surpasses the SA-CB binder system (3.35 V) and SA binder system (below 3.3 V)-based electrodes. The further evidence for the improvement of mechanical property, electronic and lithium ion conductivity are elaborated in the following sections. The self-discharge behavior of the resultant LFP cells was investigated as shown in Supporting Information Figure S5. Generally, the extent of self-discharge is increasing monotonically with storage time and temperature. The self-discharge test on LFP@SA-PProDOT cell is conducted at 55 °C at full charge state. As indicated in Supporting Information Figure S5, the discharge capacity gradually decreased to ca. 130 mAh/g after 7 weeks storage at 55 °C, that is, ca. 5% lost per month, which meets the commercial requirements. In fact, this performance is still remarkable among LFP cells at 55 °C.49,50 The electronic conductivity and conducting mechanism can be experimentally verified and explored by cyclic voltammetry (CV) tests on SA-PProDOT, and SA thin films under a mimic condition of anodes in a lithium-ion environment, respectively (see Supporting Information Figure S6). The profile of SAPProDOT suggests an in situ lithium doping at ca. 2.5 V (Li/ Li+), which can intrinsically improve the electronic conductivity. 51 The reversible redox peaks of SA and ProDOT demonstrate the stability of the polymers with functional groups.[4,52] The improvement on electronic conductivity through the lithium ion doping is quantitatively evaluated by the electrochemical impedance spectroscopy (EIS) measurements. The EIS profiles of different binder samples are collected as shown in Figure 4a and b. The plot includes the real component of impedance on the horizontal axis (Z') and the imaginary component of the impedance on the vertical axis (Z''). It is well-established that the lithium ion migration resistance (Rs) through the multilayer surface films

and the charge transfer resistance (Rct) are represented by the intersection on x axis and the diameters of the semicircles in the profiles, respectively. The parameters of impedance spectra is simulated and fitted with an equivalent circuit by ZView software. All the binders share similar Rs values due to the use of identical electrolyte solution. In contrast, the Rct of LFP@SA-PProDOT sample is significantly lower than that of LFP@SA-CB, LFP@SA, and LFP@PVDF-CB samples. The Warburg coefficient σ_w can be calculated by eq 1

$$|Z'| = R_s + R_{ct} + \sigma_w \omega^{-0.5} \quad (1)$$

In addition, the plot of Z' vs the reciprocal square roots of the lower angular frequencies is shown in Supporting Information Figure S7. The slope of the fitted line is the Warburg coefficient σ_w. The calculated value of σw for LFP@ SA-PProDOT, LFP@SA-CB, LFP@SA, and LFP@PVDF-CB is 24.9, 41.2, 47.3, and 36.4, respectively (Figure 4b). Because diffusion coefficient of Lithium ion is inversely proportional to Warburg coefficient σ_w as shown in eq 2

$$D_{Li} = \frac{R^2T^2}{2n^4F^4c^2\sigma^2} \quad (2)$$

where R and T are the gas constant and temperature, respectively, and n and F are the charge transfer number and Faraday constant, respectively. c and σ are concentration of lithium and Warburg coefficient, respectively. The LFP@SAPProDOT has the largest DLi among the three electrodes. The specific conductivity of CB is typically in the range from 0.1 to 100 S/cm,[53] but both the particles and particle to particle connections for electron transport are rigid. CB composite tends to lose electronic conductivity because of ca. 6.8% volume shrinkage after delithiation for LFP particles. Therefore, such moderate improvement in conductivity of SA-PProDOT binder over that of the nonconductive polymer binder has led to great progress of the LFP electrode performances (Supporting Information Figure S8).[54,55] High ionic conductivity bestows rapid lithiation/delithiation processes especially for the LFP electrode with high impedance value. Diffusion properties of Li ions determine some of the key performance metrics of LIBs, including the lithiation/ delithiation current, practical capacity, and cycling stability.[56,57] In a polymer binder system, higher uptake of the electrolyte in polymer will facilitate a more efficient diffusivity of Li-ions, which will result in a higher charge/discharge rate performance.[52,58] The enhanced electrolyte uptake is beneficial to Liion transportation in the electrode. Though much efforts have been devoted to manipulating the diffusivity in cathode materials, no significant breakthrough in ionic conductivity have been achieved. As shown in Figure 4c, when SA swells in the electrolyte solution, the total electrolyte uptake is ca. 11.5 wt % of its final weight. The electrolyte uptake is tripled for SAPProDOT, accounting for ca. 32%, which is significantly higher than PVDF (ca. 24%) in the electrolyte. The larger electrolyte uptake is due to the increased polarity of the polymer, which is induced by the attachment of ProDOT groups.4,5 Also, the uniform distribution of the synthesized ether moieties in the SA-PProDOT binder helps to increase the polarity and so the overall electrolyte uptake capacity.

In addition to the promoted ionic conductivity, improved electrode mechanical stability and adhesion among the laminate, current collector, and LFP particles are other benefits associated with the modification.4,5 The binding capacity of different binders is comparatively measured using the peel test. The profiles of the peel test in Figure 4d show that SAPProDOT binder-based electrode can tolerate higher peel force (ca. 1.8 pound) than that of SA (ca. 1.6 pound) and PVDF (ca. 1.4 pound). This clearly shows that the adhesion capacity of the SA-PProDOT binder is stronger than the SA and PVDF binder systems. The existence of the multiple function groups including carboxyl, hydroxyl, and ester in SA-PProDOT can promote the chemical bonding among the active materials,

which results in the stronger binding capability.

The mechanical hardness of the resultant laminates are quantitatively measured using nanoscratch and nanoindentation tests. In the nanoscratch test, average friction coefficient using the same indenter and normal force suggests stronger mechanical integrity. The normal force in the scratch test is set to 500 μN and the scratch length is set to 12 μm. During the scratch tests, lateral force is recorded in real-time and the friction coefficient is calculated from it with known applied normal force, as shown in Figure 5a. The average friction coefficient of LFP@SA-PProDOT electrode is higher than that of CMC, suggesting the higher binding capability of the SAPProDOT polymer. Moreover, the friction coefficient of LFP@SA-PProDOT remains more constant along with the whole scratch process. This implies the better homogeneity of the SAPProDOT binder system-based electrode. As shown in Figure 5c and d, the scanning probe microscopy (SPM) visually verifies the uniformity of the electrodes. The 3D in situ scratch track on the LFP@SA electrode surface is broader and more dispersive than that of the LFP@SA-PProDOT.59

Besides friction coefficient, the hardness of electrodes can be evaluated by nanoindentation tests. The higher hardness of the electrodes indicates the better binding capability and stability during the operation of LIBs. Nanoindentation tests on LFP@SA-PProDOT and LFP@SA electrodes are undertaken with the force of 500 μN and 1000 μN. When the loading force is set as 1000 μN, the indentation depth is ca. 1200 and 700 nm for LFP@SA and LFP@SA-PProDOT electrodes, respectively. The same trend can be found when the loading force is 500 μN in Figure 5b. Overall, indentation tests demonstrate that the LFP@SA-PProDOT electrode is around two times stronger than LFP@SA electrode.

The mechanical property under electrolyte environment is critical to the electrode integrity and diffusion ability. Hence, the scratch and indentation tests after impregnation in electrolyte were performed as shown in Supporting Information Figure S9. The friction coefficient of the LFP@SA-PProDOT appears an insignificant decrease in strong contrast with the significant decline of the LFP@SA-CB electrode. The indentation profile in Supporting Information Figure S9b indicates that the impregnation of electrolyte results in 300 nm deeper “dent” of the LFP@SA-CB sample than that of LFP@SA-PProDOT, suggesting that LFP@SA-PProDOT sample has a remarkably better mechanical strength than LFP@SA-CB sample in the presence of electrolyte. In addition to the mechanical test of the laminate, the nanoindentation test was carried out on the polymer binders under the force of 2000 μN and ten individual indents were adopted for accurate calculations. The indentation depth (Er), given in eq 3, is a combined modulus of the indenter and specimen

$$\frac{1}{E_r} = \frac{(1-\nu^2)}{E} + \frac{(1-\nu'^2)}{E'} \qquad (3)$$

where E and ν are the Young’s modulus and Poisson’s ratio of the specimen, respectively, and E' and ν' are the elastic modulus and Poisson’s ratio of the indenter, respectively. For a standard diamond indenter, E' is 1140 GPa and ν' is 0.07. The trend of the reduced modulus value Er is presented in Supporting Information Figure S10. The average modulus of the SA-PProDOT polymer is higher than SA, suggesting a better binding strength, which is beneficial for delamination tolerance to achieve long cycle life. In summary, cyclohexane/DBSA/water microemulsion system facilitates the esterification reaction between SA and ProDOT molecules at the cyclohexane/water interface while it protects the hydrophilic groups (such as carboxylate groups) in SA framework, leading to formation of a multifunctional polymer binder SA-PProDOT. The SA-PProDOT demonstrates significantly better binding capability, mechanical property, electrolyte uptake, lithium ion diffusion coefficient, and electronic conductivity when compared with either SA or CMC. The optimized performances of our SA-PProDOT binder, when compared with SA, SA

plus CB, and PVDF plus CB, show that our new polymer has improved mechanical properties, Li-ion conduction, diffusion efficient, and lower electrochemical impedance. Due to the conjugated network of the PProDOT and the lithium doping under the battery environment, the SA-PProDOT becomes conductive and matches the conductivity required for LFP LIBs. Without the need of conductive additives such as carbon black, the theoretical specific capacity ca. 170 mAh/g has been achieved at C/10. Besides the advantage of the use of naturally occurring polymers, the proposed synthesis method is an exciting and promising way for production of LIB binders at low cost and in environmentally benign way.

ACKNOWLEDGMENTS

This work is supported by the Australia Research Council and by the Batteries for Advanced Transportation Technologies (BATT) Program at Lawrence Berkeley National Laboratory. The synthesis of polymer binders was conducted in Institute for Glycomics, Griffith University. Electron microscopy experiments are conducted at the Centre for Microscopy & Microanalysis (CMM), located at the University of Queensland.

ABBREVIATIONS

LIBs, lithium ion batteries; LFP, LiFePO4; EVs, electric vehicles; SA, sodium alginate; ProDOT, 3,4-propylenedioxythiophene-2,5-dicarboxylic acid; PProDOT, poly(3,4-propylenedioxythiophene); CMC, carboxymethyl cellulose; PVDF, polyvinylidene difluoride; DBSA, dodecyl benzenesulfonic acid; EC, ethylene carbonate; DMC, dimethyl carbonate; CV, cyclic voltammetry; SEM, scanning electron microscope; XRD, X-ray diffraction; XPS, X-ray photoelectron spectroscopy; SPM, canning probe microscopy; FTIR, Fourier transform infrared spectroscopy; EIS, electrochemical impedance spectroscopy

REFERENCES

(1) Goodenough, J. B.; Kim, Y. Chem. Mater. 2010, 22 (3), 587−603.
(2) Etacheri, V.; Marom, R.; Elazari, R.; Salitra, G.; Aurbach, D. Energy Environ. Sci. 2011, 4 (9), 3243−3262.
(3) Myers, V. S.; Weir, M. G.; Carino, E. V.; Yancey, D. F.; Pande, S.; Crooks, R. M. Chem. Sci. 2011, 2 (9), 1632−1646.
(4) Wu, M.; Xiao, X.; Vukmirovic, N.; Xun, S.; Das, P. K.; Song, X.; Olalde-Velasco, P.; Wang, D.; Weber, A. Z.; Wang, L.-W.; Battaglia, V. S.; Yang, W.; Liu, G. J. Am. Chem. Soc. 2013, 135 (32), 12048−12056.
(5) Liu, G.; Xun, S.; Vukmirovic, N.; Song, X.; Olalde-Velasco, P.; Zheng, H.; Battaglia, V. S.; Wang, L.; Yang, W. Adv. Mater. 2011, 23 (40), 4679−4683.
(6) Ryou, M. H.; Kim, J.; Lee, I.; Kim, S.; Jeong, Y. K.; Hong, S.; Ryu, J. H.; Kim, T. S.; Park, J. K.; Lee, H.; Choi, J. W. Adv. Mater. 2013, 25 (11), 1571−1576.
(7) Wang, C.; Wu, H.; Chen, Z.; McDowell, M. T.; Cui, Y.; Bao, Z. Nat. Chem. 2013, 5 (12), 1043−1049.
(8) Liu, N.; Lu, Z.; Zhao, J.; McDowell, M. T.; Lee, H.-W.; Zhao, W.; Cui, Y. Nat. Nanotechnol. 2014, 9 (3), 187−192.
(9) Wang, H.; Yang, Y.; Liang, Y.; Cui, L.-F.; Casalongue, H. S.; Li, Y.; Hong, G.; Cui, Y.; Dai, H. Angew. Chem., Int. Ed. 2011, 50 (32), 7364−7368.
(10) Song, J.; Zhou, M.; Yi, R.; Xu, T.; Gordin, M. L.; Tang, D.; Yu, Z.; Regula, M.; Wang, D. Adv. Funct. Mater. 2014, 24 (37), 5904−5910.
(11) Seh, Z. W.; Zhang, Q.; Li, W.; Zheng, G.; Yao, H.; Cui, Y. Chem. Sci. 2013, 4 (9), 3673−3677.
(12) Kovalenko, I.; Zdyrko, B.; Magasinski, A.; Hertzberg, B.; Milicev, Z.; Burtovyy, R.; Luzinov, I.; Yushin, G. Science 2011, 334 (6052), 75−79.

(13) Li, J.; Lewis, R. B.; Dahn, J. R. Electrochem. Solid-State Lett. 2007, 10 (2), A17−A20.
(14) Buqa, H.; Holzapfel, M.; Krumeich, F.; Veit, C.; Novak, P. J. Power Sources 2006, 161 (1), 617−622.
(15) Li, C.-C.; Wang, Y.-W. J. Electrochem. Soc. 2011, 158 (12), A1361−A1370.
(16) Zhao, Y.; Peng, L.; Liu, B.; Yu, G. Nano Lett. 2014, 14 (5), 2849−2853.
(17) Shin, H. C.; Cho, W. I.; Jang, H. Electrochim. Acta 2006, 52 (4), 1472−1476.
(18) Amine, K.; Liu, J.; Belharouak, I. Electrochem. Commun. 2005, 7 (7), 669−673.
(19) Hu, Y.-S.; Guo, Y.-G.; Dominko, R.; Gaberscek, M.; Jamnik, J.; Maier, J. Adv. Mater. 2007, 19 (15), 1963−1966.
(20) Wang, Y.; Wang, Y.; Hosono, E.; Wang, K.; Zhou, H. Angew. Chem., Int. Ed. 2008, 47 (39), 7461−7465.
(21) Wang, L.; He, X.; Sun, W.; Wang, J.; Li, Y.; Fan, S. Nano Lett. 2012, 12 (11), 5632−5636.
(22) Zhang, X.; van Hulzen, M.; Singh, D. P.; Brownrigg, A.; Wright, J. P.; van Dijk, N. H.; Wagemaker, M. Nano Lett. 2014, 14 (5), 2279−2285.
(23) Zhao, Y.; Peng, L.; Liu, B.; Yu, G. Nano Lett. 2014, 14 (5), 2849−2853.
(24) Xun, S.; Xiang, B.; Minor, A.; Battaglia, V.; Liu, G. J. Electrochem. Soc. 2013, 160 (9), A1380−A1383.
(25) Fei, H.; Peng, Z.; Yang, Y.; Li, L.; Raji, A.-R. O.; Samuel, E. L. G.; Tour, J. M. Chem. Commun. 2014, 50 (54), 7117−7119.
(26) Shinde, U. A.; Nagarsenker, M. S. Indian J. Pharm. Sci. 2009, 71 (3), 313−317.
(27) Sadecka, E.; Szelag, H. J. Surfactants Deterg. 2013, 16 (3), 305−315.
(28) Zoumpanioti, M.; Stamatis, H.; Xenakis, A. Biotechnol. Adv.2010, 28 (3), 395−406.
(29) Jing, L.; Li, X. J.; Han, Y. C.; Chu, Y. Colloid Sur., A 2008, 326 (1−2), 37−41.
(30) Zong, K. W.; Madrigal, L.; Groenendaal, L.; Reynolds, J. R.Chem. Commun. 2002, 21, 2498−2499.
(31) Gaupp, C. L.; Welsh, D. M.; Reynolds, J. R. Macromol. Rapid Commun. 2002, 23 (15), 885−889.
(32) Kim, J.-M.; Park, H.-S.; Park, J.-H.; Kim, T.-H.; Song, H.-K.; Lee, S.-Y. ACS Appl. Mater. Interfaces 2014, 6 (15), 12789−12797.
(33) Yang, Y.; Yu, G.; Cha, J. J.; Wu, H.; Vosgueritchian, M.; Yao, Y.; Bao, Z.; Cui, Y. ACS Nano 2011, 5 (11), 9187−9193.
(34) Shao, D.; Zhong, H.; Zhang, L. ChemElectroChem 2014, 1 (10), 1679−1687.
(35) Das, D.; Das, P. K. Langmuir 2003, 19 (22), 9114−9119.
(36) Jenta, T. R. J.; Batts, G.; Rees, G. D.; Robinson, B. H. Biotechnol. Bioeng. 1997, 54 (5), 416−427.
(37) Avramiotis, S.; Stamatis, H.; Kolisis, F. N.; Lianos, P.; Xenakis, A. Langmuir 1996, 12 (26), 6320−6325.
(38) Kuss, C.; Lepage, D.; Liang, G.; Schougaard, S. B. Chem. Sci. 2013, 4 (11), 4223−4227.
(39) Chung, S. Y.; Chiang, Y. M. Electrochem. Solid-State Lett. 2003, 6 (12), A278−A281.
(40) Jiang, J.; Dahn, J. R. Electrochem. Commun. 2004, 6 (1), 39−43.
(41) Herle, P. S.; Ellis, B.; Coombs, N.; Nazar, L. F. Nat. Mater. 2004, 3 (3), 147−152.
(42) Bai, P.; Cogswell, D. A.; Bazant, M. Z. Nano Lett. 2011, 11 (11), 4890−4896.
(43) Chueh, W. C.; El Gabaly, F.; Sugar, J. D.; Bartelt, N. C.; McDaniel, A. H.; Fenton, K. R.; Zavadil, K. R.; Tyliszczak, T.; Lai, W.; McCarty, K. F. Nano Lett. 2013, 13 (3), 866−872.
(44) Amin, R.; Lin, C.; Peng, J.; Weichert, K.; Acartuerk, T.; Starke, U.; Maier, J. Adv. Funct. Mater. 2009, 19 (11), 1697−1704.
(45) Bouafif, H.; Koubaa, A.; Perre, P.; Cloutier, A.; Riedl, B. J. Wood Chem. Technol. 2008, 28 (4), 296−315.
(46) Chatjigakis, A. K.; Pappas, C.; Proxenia, N.; Kalantzi, O.; Rodis, P.; Polissiou, M. Carbohydr. Polym. 1998, 37 (4), 395−408.
(47) Morris, N. M.; Catalano, E. A.; Andrews, B. A. K. Cellulose 1995, 2 (1), 31−39.
(48) Wei, Z.; Han, H.; Filatov, A. S.; Dikarev, E. V. Chem. Sci. 2014, 5 (2), 813−818.

(49) Utsunomiya, T.; Hatozaki, O.; Yoshimoto, N.; Egashira, M.; Morita, M. J. Power Sources 2011, 196 (20), 8598−8603. (50) Hausbrand, R.; Becker, D.; Jaegermann, W. Prog. Solid State Chem. 2014, 42 (4), 175−183.
(51) Li, A.; Lu, R.-F.; Wang, Y.; Wang, X.; Han, K.-L.; Deng, W.-Q. Angew. Chem., Int. Ed. 2010, 49 (19), 3330−3333.
(52) Park, M.; Zhang, X.; Chung, M.; Less, G. B.; Sastry, A. M. J. Power Sources 2010, 195 (24), 7904−7929.
(53) Kassim, S. A. E.; Achour, M. E.; Costa, L. C.; Lahjomri, F. J. Electrost. 2014, 72 (3), 187−191.
(54) Liu, X.-m.; Yan, P.; Xie, Y.-Y.; Yang, H.; Shen, X.-d.; Ma, Z.-F. Chem. Commun. 2013, 49 (47), 5396−5398.
(55) Yu, X.; Wang, Q.; Zhou, Y.; Li, H.; Yang, X.-Q.; Nam, K.-W.; Ehrlich, S. N.; Khalid, S.; Meng, Y. S. Chem. Commun. 2012, 48 (94), 11537−11539.
(56) Wang, C.; Hong, J. Electrochem. Solid-State Lett. 2007, 10 (3), A65−A69.
(57) Ma, J.; Wang, C.; Wroblewski, S. J. Power Sources 2007, 164 (2), 849−856.
(58) Kang, B.; Ceder, G. Nature 2009, 458 (7235), 190−193.
(59) Ling, M.; Xu, Y.; Zhao, H.; Gu, X.; Qiu, J.; Li, S.; Wu, M.; Song, X.; Yan, C.; Liu, G.; Zhang, S. Nano Energy 2015, 12, 178−185.

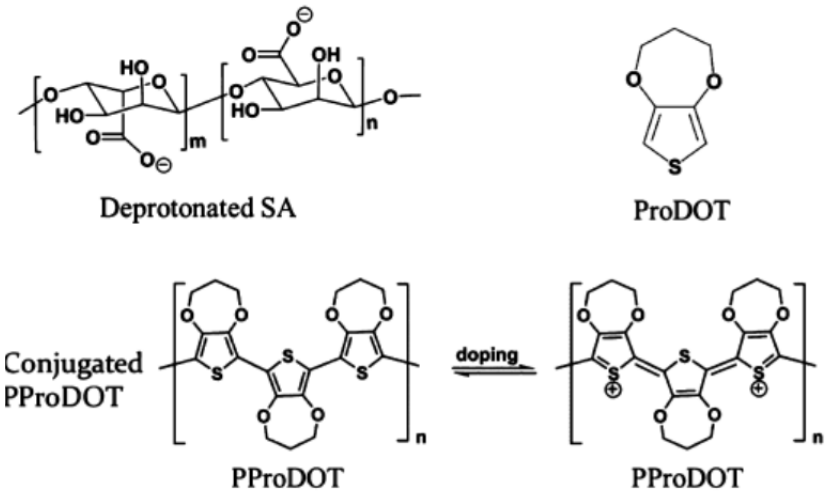

Scheme 1. Chemical structure of deprotonated sodium alginate (SA), 3,4-propylenedioxythiophene-2,5-dicarboxylic acid (ProDOT), and poly(3,4-propylenedioxythiophene) (PProDOT)

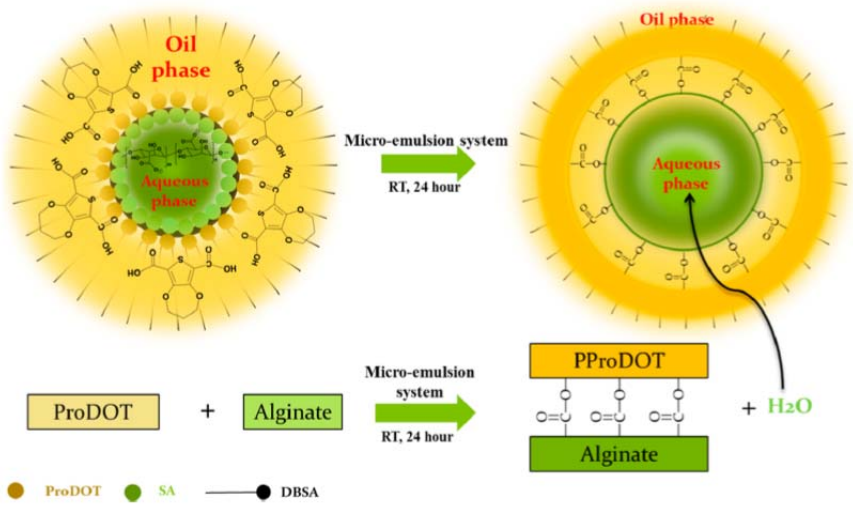

Figure 1. Schematic design of the microemulsion system for synthesis of SA-PProDOT polymer. SA and ProDOT molecules self-assemble along with hydrophilicity of the functional groups, forming an interface where the esterification reaction takes place. The produced water is removed from the interface to the hydrophilic phase, which advances the reaction equilibrium forward.

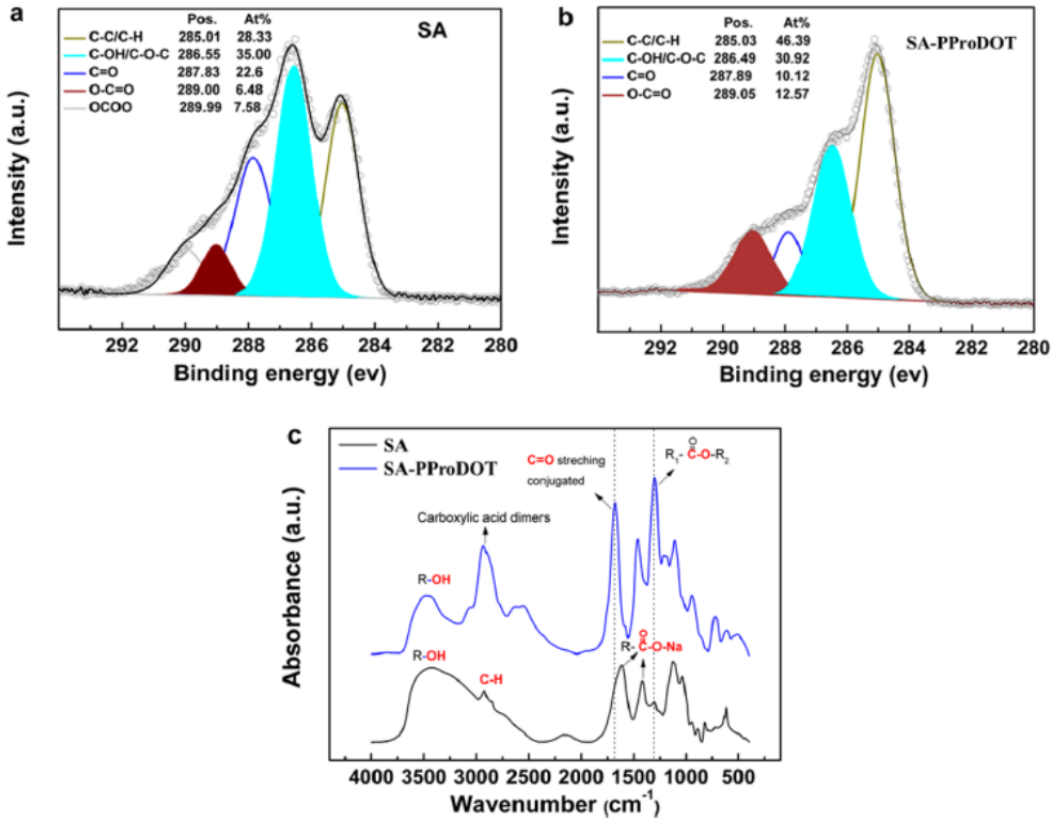

Figure 2. XPS spectra of (a) SA and (b) SA-PProDOT and (c) FTIR spectra of SA and SA-PProDOT polymers.

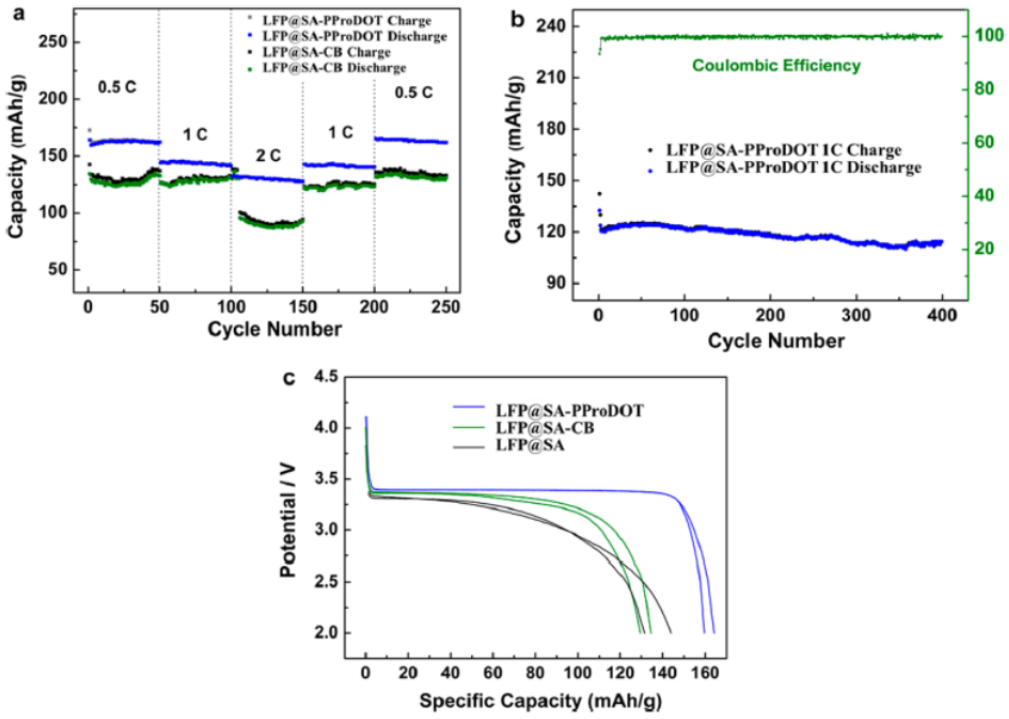

Figure 3. (a) Rate performance of the electrodes based on SA-PProDOT (LFP:binder = 8:2) and SA plus CB (LFP:PVDF:CB = 8:1:1). (b) Long term performance of LFP electrodes binder based on SA-PProDOT (LFP:binder = 8:2) binder. (c) Galvanostatic discharge profile of LFP electrodes based on SA-PProDOT (LFP:binder = 8:2), SA (LFP binder = 8:2), and SA plus CB (LFP:PVDF:CB = 8:1:1) binders between the cycling voltage of 2.0 and 4.2 V.

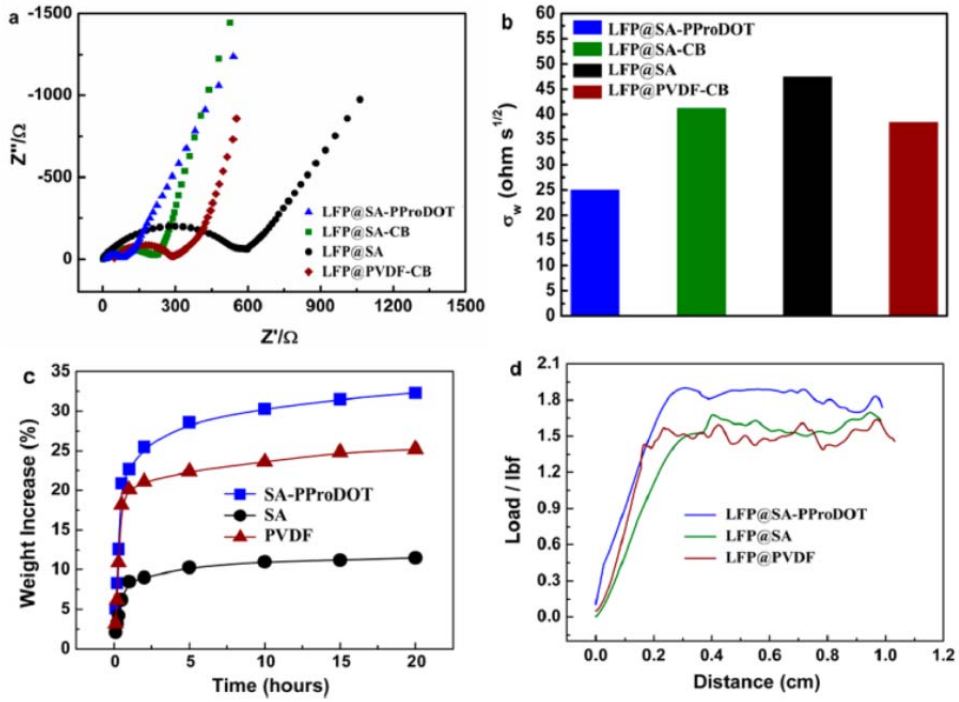

Figure 4. (a) EIS spectra of the LFP@SA-PProDOT, LFP@SA-CB, LFP@SA, and LFP@PVDF-CB samples between 0.1 Hz and 100 kHz. (b) Warburg Coefficient of LFP@SA-PProDOT, LFP@SA-CB, LFP@SA, and LFP@PVDF-CB samples. (c) Swelling tests of SA-PProDOT, SA, and PVDF film in the 1 M LiPF6 EC/DEC (1:1) electrolyte. (d) Peeling test of LFP@SA-PProDOT, LFP@SA, and LFP@PVDF samples.

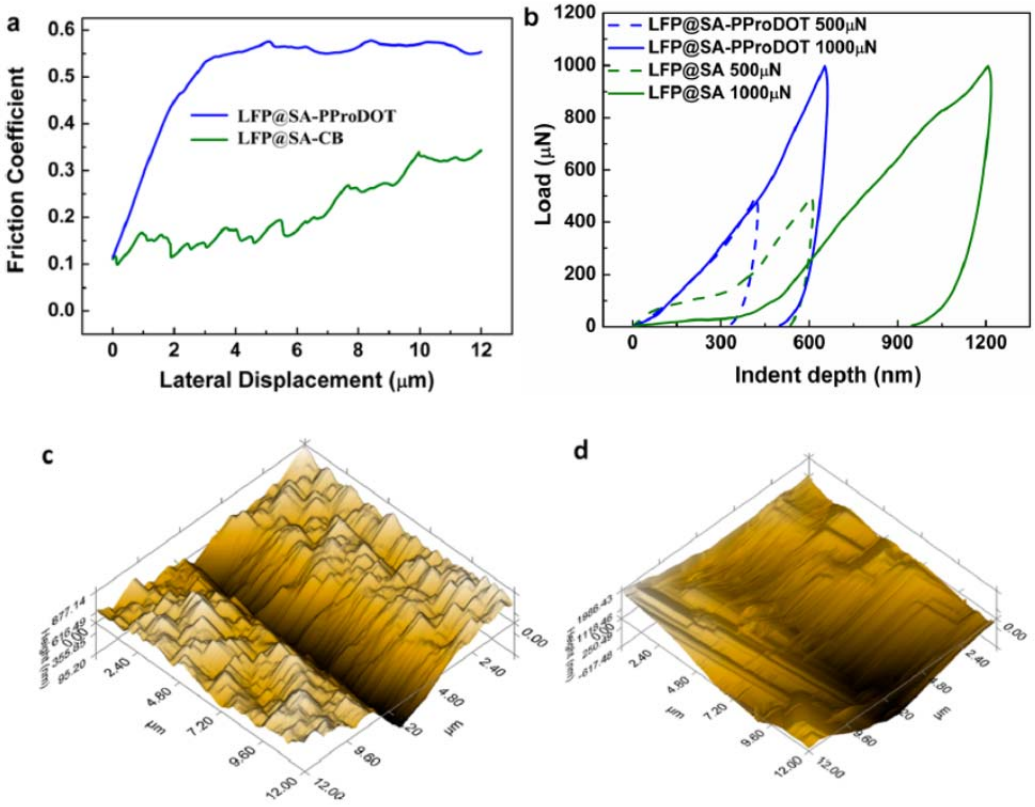

Figure 5. (a) Peel test of LFP@SA-PProDOT and LFP@SA-CB electrodes. (b) Nanoscratch and indentation tests for LFP@SA-PProDOT and LFP@SA-CB electrodes. (c) 3D in situ SPM image of LFP@SA-PProDOT after nanoscratch tests. (d) 3D in situ SPM image of LFP@SA-CB electrode after nanoscratch tests.